Performance of Echidna fiber positioner for FMOS on Subaru

Masayuki Akiyama[a,b], Scott Smedley[c], Peter Gillingham[c], Jurek Brzeski[c], Tony Farrell[c], Masahiko Kimura[b], Rolf Muller[c], Naoyuki Tamura[b], and Naruhisa Takato[b]

[a]Astronomical Institute, Tohoku University, Aramaki, Aoba-ku, Sendai, 980-8578, Japan;
[b]Subaru Telescope, NAOJ, 650 North Aohoku Place, Hilo, HI, 96720, USA;
[c]Anglo-Australian Observatory, PO Box 196, Epping, NSW 2117, Australia

ABSTRACT

Echidna is a fiber positioner designed and built by the Anglo-Australian Observatory using novel technology to position 400 fibers in the prime focus field of the Subaru telescope. The fibers feed two near infrared OH-suppression spectrographs, the whole project being known as Fiber Multi Object Spectrograph (FMOS). In order to accommodate the large number of the fibers in the physically limited area, a new fiber positioning method is developed. Stand-alone tests of the positioner at sea level confirm its performance is fully satisfactory. Initial results and prospects of the on-sky commissioning tests of the positioner are also described.

Keywords: fiber positioner, piezoelectric actuators, Subaru telescope

1. INTRODUCTION

The Fiber Multi-Object Spectrograph (FMOS) is a next generation near-infrared spectrograph for the 8.2m Subaru telescope, being able to obtain spectra of 400 objects simultaneously.[1,2] Echidna is the fiber positioning system for the instrument and is attached to the prime-focus. The focus has $30'$ diameter FoV with the physical size of 150mm diameter. In order to position 400 fibers in the limited area, a new fiber positioning method, tilting a fiber attached to a carbon-fiber "spine" sitting on a ball mount with a quadrant tube piezo actuator, was developed. See Fig. 1. Once saw-tooth signal is applied to the piezo actuator, the spine tilts due to a slippage of the pivot ball against the three point mount. The prototyping stage of the positioner is described in Gillingham et al.[3] and in Moore et al.[4] The overall mechanical design is shown in Gilligham et al.,[5] and its details are described in Brzeski et al.[6] See Fig. 4 of Ref.6 for the input signal and the movement. The 400 fibers feed two cooled OH-suppression spectrographs, one developed in Kyoto university[7,8] and the other build in UK.[9,10] Both of them cover 900-1800nm. In the fiber train, there is a collimated light coupling,[11,12] in order to convert the fast F/2 ratio of the prime focus, and to detach the positioner from the telescope.

In this paper, we describe the results of stand-alone and on-sky evaluations of the novel fiber positioning system. Most of the stand-alone tests were performed in the Hilo base facility at sea-level. They were done either on a custom tilting jig or in the prime-focus unit enclosed in a tilting frame. The whole positioner unit on the tilting jig is shown in the left panel of Fig. 2. The installation process to the prime-focus unit is shown in the right panel. The stand-alone tests confirmed the performance of the positioner was fully satisfactory. Measured mechanical properties of each component of the fiber positioner unit are summarized in Section 2. Dynamical properties of the positioner and the results of fiber positioning tests are described in Section 3. After careful transfer to the Mauna Kea summit facility, we confirmed that the performance did not degrade in the low temperature and low humidity environment. On-sky commissioning was conducted Dec. 2007, Jan. and May. 2008, and scheduled for Jun. and Aug. 2008. The initial results of the commissioning and prospects are summarized in Section 4.

There are precise requirements for the accuracy of the fiber positioning. In order to minimize the loss of the coupling efficiency due to the misalignment between a target and a fiber, the fiber must be positioned within 20μm of the target. During the concept design study, the optimal core size of the science-fibers was determined to be $1.2''$, which corresponds to 100μm at the prime-focus, maximizing the expected SN ratios of faint galaxies

Further author information: (Send correspondence to M.A.)
M.A.: E-mail: akiyama@astr.tohoku.ac.jp

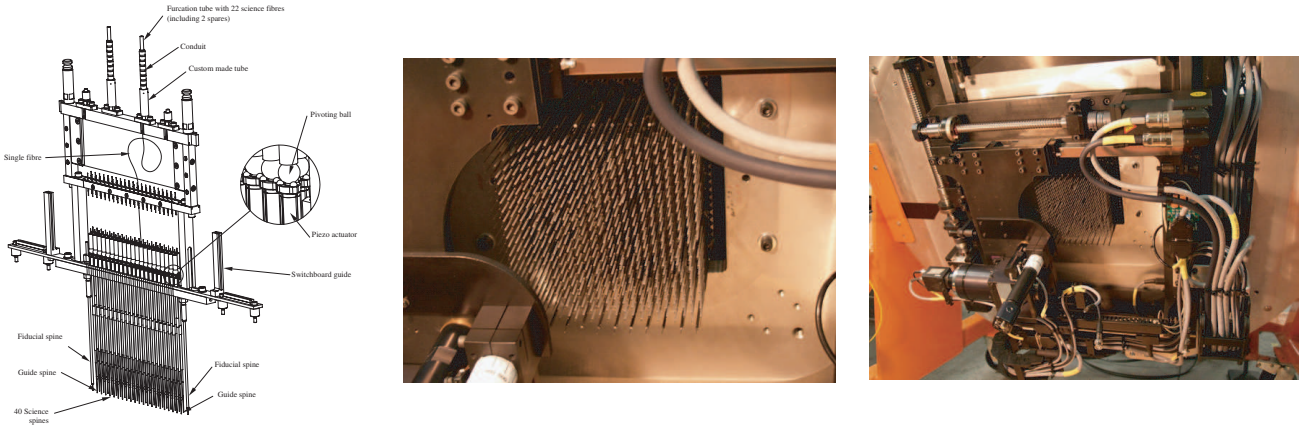

Figure 1. Left) drawing of one module of the fiber positioner from Fig. 4 of Ref6. One module has 20×2 science-fibers and 2 guide-bundles at both ends of the module. Science-fibers are 100μm diameter core fiber, and guide-bundles are bundles of 7 50μm-core fibers with 80μm spacing, which corresponds to 0.96″ at the focal plane. A fiber is attached to a carbon-fiber tubing, called "spine", with a pivoting ball and a tungsten counter weight. The pivoting ball is sitting on a three-point mount with a ring magnet at the top of a quadrant tube piezo actuator. Spines for the science-fibers and the guide-bundles have the same structure. Middle) close up view of the focal plane. 12 modules of the 40 science-fibers cover the FoV. 400 science-fibers within the 30′ diameter FoV are connected to the spectrographs. The spacing between neighboring spines is 7mm. Each spine is designed to be able to reach the home positions the 6 neighboring spines. Right) structure of the Echidna unit around the focal plane. The positions of the tips of the fibers are measured with the fiber camera of the Focal Plane Imager (FPI) on the XY gantry.

in the background limited condition. In Fig. 3, the coupling efficiency of the 100μm fiber to a stellar object is shown as a function of misalignment. For misalignment less than 20μm (=0.24″) the reduction of the coupling efficiency is less than 10%, even under a good seeing condition with FWHM=0.5″.

Due to a number of physical effects (including the changing contact position of the pivot ball with the three-point mounts) the repeatability of spine movement is not precise. In order to achieve the required positioning accuracy, we need to iterate. After one movement, the positions of the tips of the fibers are re-measured with the spine camera. In order to position the 400 fibers within a reasonable time, 10-15 minutes, the maximum number of iterations is ∼7. Each iteration process takes approximately 100 seconds. If the worst-case fiber movement has 40% accuracy in each operation, 10μm positioning accuracy can be achieved with 7 iterations for movement from the home position to the edge of the patrol field: $0.4^7 \times 7200\mu\text{m} \sim 10\mu\text{m}$.

2. MECHANICAL PROPERTIES

2.1 Accuracy of the measurements of the fiber positions

Accurate measurements of the fiber positions are critical to the evaluations of the mechanical and dynamical properties of the positioner. The positions are measured with the spine camera of the Focal Plane Imager (FPI). The camera covers the entire focal plane by moving with an XY gantry. Each fiber can be back-illuminated individually by a illumination mechanism with a prism at the connector end of the fibers (inside the black box shown in the left panel of Fig. 2). The spine camera has 768×493 physical pixels with an 11μm×13μm pixel size and covers the 400 fibers with 59 FoVs (see Fig. 9 of Ref. 5). The positions of the 400 fibers can be sequentially measured in approximately 100 seconds.

The spine-camera uses a telecentric lens to image the spine tips. The distortion pattern of the spine-camera and the non-orthogonality of the XY gantry were calibrated by measuring a grid-pattern light-source attached at the focal plane instead of the fiber modules. In details of the calibration source, see Section 1.2.3 of Ref.6. In order to evaluate the effect of gravity on the non-orthogonality, the calibrations were done at various tilt angle and the rotator angle inside the prime focus unit. The distortion pattern of the spine-camera was described well with a model including up to the third order term; the residuals of the model is 1.3μm RMS with a maximum

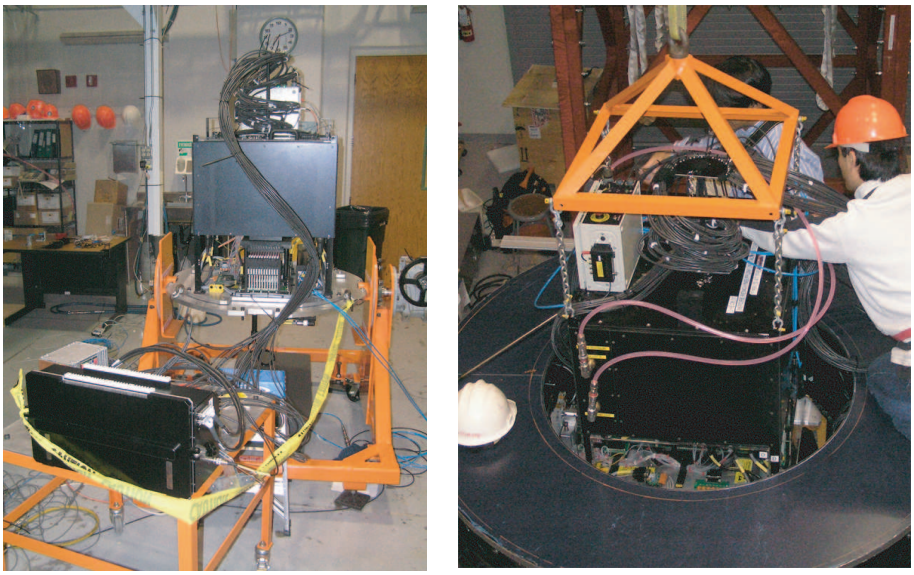

Figure 2. Left) Echidna unit on the testing jig (orange frame structure). The bottom of the unit corresponds to the focal plane. The black box on the table in front of the unit is the fiber connector assembly. Right) Echidna under installation into the prime-focus unit. The installation is done off the telescope in the prime-focus unit storage area and attached to the telescope, Echidna being enclosed in the unit.

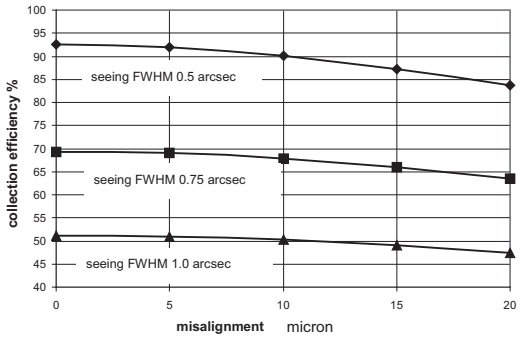

Figure 3. Plots of percentage energy encircled within a 100μm diameter circle as a function of misalignment for three different seeing conditions.

error of 3.1μm. The residuals are shown in the left panel of Fig. 4. The non-orthogonality of the XY gantry can be described well with the mean parameters determined by averaging the parameters measured at various tilt and rotator angles. The residuals of the calibrations are 2.0μm RMS in the entire FoV, including both residuals of the distortion pattern and the non-orthogonality models. The RMS represents the accuracy of the fiber position measurements. The residuals do not have systematic component as shown in the middle panel of Fig. 4.

Additionally, repeatability of the measurements were checked by measuring the positions of the fibers multiple times using the spine-camera. The results are shown in the right panel of Fig. 4. The differences of the measured positions between two independent measurements have a scatter of 1μm RMS (p-p about $\pm$2μm) for each direction. If we measure a position of a fiber in multiple times without moving the spine camera, the resultant scatter in each direction is $\sim$1μm RMS. Thus, the scatter of the positions in the multiple-measurements is dominated by the accuracy of the centroid evaluation.

The above accuracy of the position measurements and the repeatability are satisfactory to confirm the positions of the fibers.

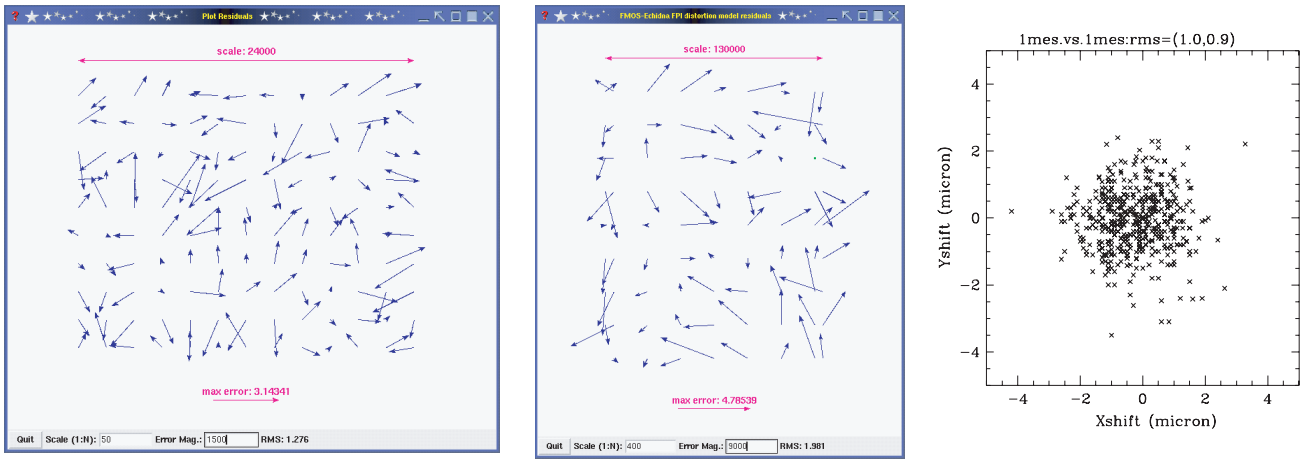

Figure 4. Left) Residuals in one FoV of the spine-camera after removing third order distortion. No systematic residual. Middle) residuals in the entire focal plane after removing the camera distortion model and the gantry XY movement non-orthogonality model. Right) The differences of the measured positions of spine tips in two measurements.

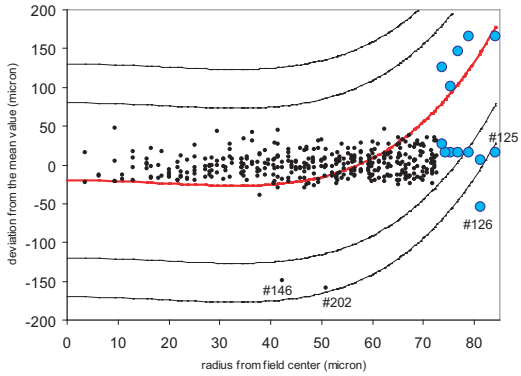

Figure 5. Results of the parfocality measurements. The black dots and blue circles represents the measurements for the science-fibers and the guide-bundles, respectively. The red solid line represent the best focus position, and the thin sold lines indicate $\pm 100\mu$m and $\pm 150\mu$m from the best focus.

2.2 Length of the spines

Due to the fast F/2 ratio of the prime-focus, careful control of the parfocality of the fibers is important. If a 100μm fibre is defocused by 150μm, the reduction of the coupling efficiency will be 5% under typical seeing condition. If an object at the edge of the patrol area of each fiber is observed, then the tip of the fiber is 162μm off from the focal plane. In order to minimize the further offset, the heights of the three point mounts from the base plate of the Echidna unit and the lengths of the spines are carefully controlled during manufacturing (in details, see Section 1.1.3 and 1.1.4 of Ref.6).

In order to check the parfocality of the tips of the fibers, a CCD camera with a high-magnification lens was attached to the FPI and a relative measurement of the best focus position was calculated. Results for all 400 science fibers and all 14 guide bundles are shown in Fig. 5 with black dots and light-blue circles, respectively. The red solid line represents the curvature of the focal plane. The vertical position of the solid line was determined so that the RMS of the deviation of the science spines from the focal plane is minimum. All but two of the science fibers are within $\pm 100\mu$m of the best focus position. The RMS of the deviation is 33μm for the science fibers. For the guide-bundles, all but two spines have length within $\pm 150\mu$m of the focus position.

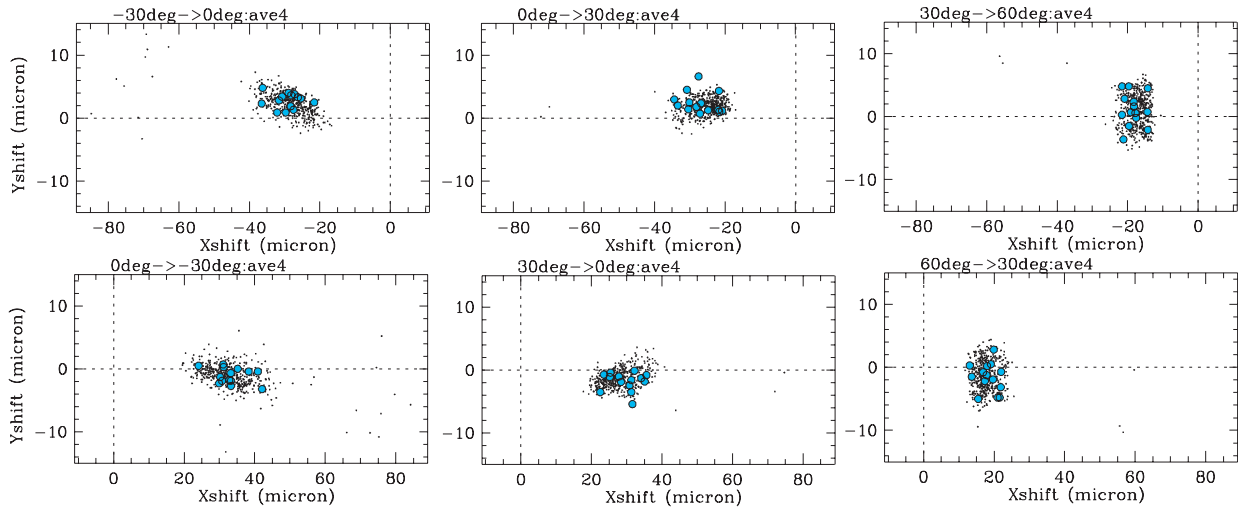

Figure 6. Variation of the positions of the tips of the science-fibers (black dots) and the guide-bundles (light-blue circles) following the change of the tilt angle. The tilt angle changes are indicated at top of the each panel. In these measurements, X-axis corresponds to the direction of gravity. Several spines show very large offset due to slippages of their pivot ball during the tilt movement.

2.3 Flexure of the spines

In order to examine the amount of flexures of the spines, we measured the movements of the tips of the fibers with changing tilt angle between 0 degrees and 60 degrees. The results are shown in Fig. 6. Black dots and light-blue circles represent the offsets of the science-fibers and guide-bundles, respectively, between two measurements before and after changing the tilt angle. The offsets reflect the variation in flexure between the two tilt angles due to gravity. The direction of gravity is in the X-direction in these panels. The change of the tilt angle is shown at the top of each panel.

The average of the absolute size of the offsets are 30μm and 20μm respectively, for the tilt angle changes of 0↔30degree (left and middle panels) and 30↔60degree (right panels). There is a $\pm$10μm scatter around the average offsets. Several spines show very large offsets; slippages of the pivot ball of the spines during the change of the tilt angle are thought to cause the large offsets of these spines. In Fig. 7, the distribution of the relative deflection of the spines from the mean deflection during the tilt angle change of 0 to 60 degree is shown as a histogram. Measurements in 4 different rotation angles are shown in different lines.

Because the offsets between the guide-bundles and the guide stars will be removed by correcting the tracking of the telescope during real observations, the average flexure of the spines will be cancelled. However, the difference between the flexure of the science-fiber and the guide-bundle spines will cause misalignment between the science-fiber and targets. The measured variations of flexure is sufficiently small to keep the targets within 10μm accuracy during an integration with 30 degree elevation change.

2.4 Fiber position stability

We examined the stability of fiber positions by measuring the positions at a 2 hours intervals. The vibration during the measurements was comparable that observed at the top ring of the telescope. No systematic shifts were observed in the measurements at tilt angles of 0 and 30 degrees. The results at tilt angle of 60 degree are shown in Fig. 8. In this measurements, systematic offset of 2μm was observed in the first 2 hours. The offset is still sufficiently small compared with the required positioning accuracy.

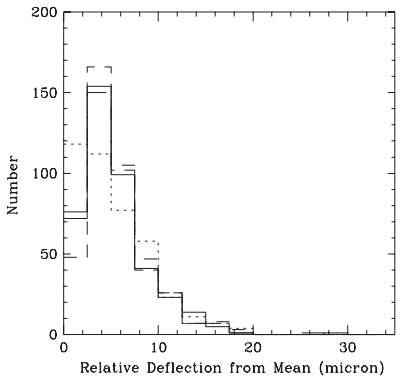

Figure 7. The magnitude of relative deflection between the tilt angle of 0 degrees to 60 degrees. Measurements at 4 different rotation angles are shown with different line types.

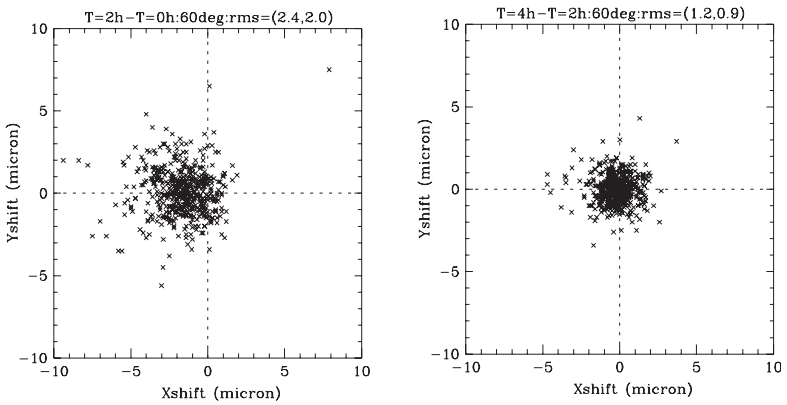

Figure 8. Fiber position stability measured at tilt angle of 60 degree. Left) Position difference in the first two hours, Right) Position difference between the two and four hours.

3. DYNAMICAL PROPERTIES

3.1 Step-size with large step numbers

The movements of the tips of the spines happen in "steps", following the input saw-tooth signal to the quadrant tube piezo (see Fig. 4 of Ref 6). There are two operation modes; the coarse and the fine modes with 140V 70Hz and 55V 15Hz saw-tooth signals, respectively. The size of each step is measured with the spine-camera at three tilt angles, 0, 30, and 60 degrees. The measured step sizes are shown in Fig. 9 for $X+$ movement. Black dots and light blue circles represent the science-fiber and the guide-bundle spines, respectively. The upper and lower panels are for the coarse and for the fine modes. The horizontal axis is the measured step size at tilt angle of 0 degree. The average step sizes are 40μm for coarse mode and 10μm for fine mode. As a result, the movement in coarse mode is 19 times faster than the movement in fine mode; it will take 2.5s and 47s to move 7mm distance in the coarse and fine modes, respectively. The step sizes have factor of 2 scatter around the average step size from spines to spines.

The vertical axis of the figure shows the difference of the step size for each spine between different tilt angles; 30 and 0 degrees for the left panels, and 60 and 0 degrees for the right panels. No systematic increase or decrease of the step sizes is observed. The variation in step size for each spine is less than 40% for most of the spines in these tilt angles. Therefore, in order to achieve the 40% accuracy for the movement, we need to calculate the required step number for each spine using the step size of each spine, but we do not need to consider the variation of the step size of each spine due to the change of the elevation angle.

In a few months timescale, there is no significant change in the step size. The long term stability of the step size will be checked in future, but it should be noted that we can calibrate the step sizes of all spines in a few

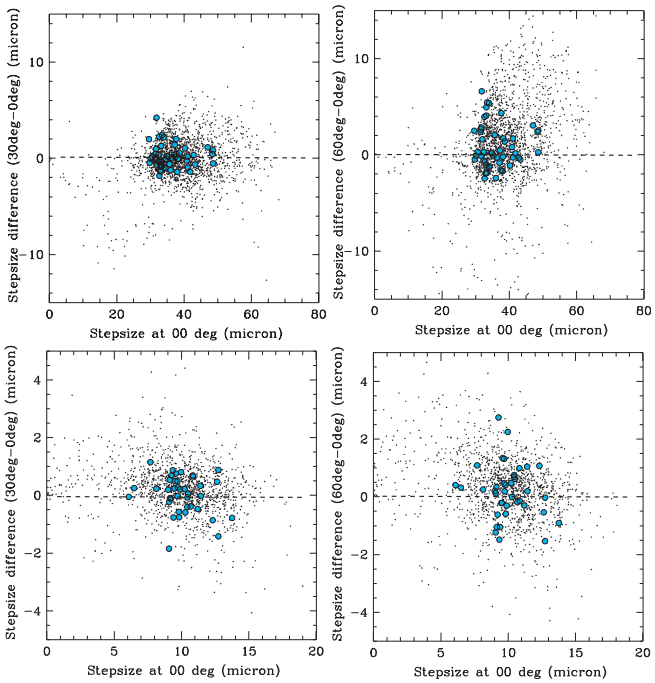

Figure 9. Step sizes measured in the X+ movement. Upper panels) for coarse mode operation. Left and right panels are for tilt angle 0 degree vs. 30 degree and 0 degree vs. 60 degree, respectively. Lower panels) for fine mode operation. Left and right panels are for tilt angle 0 degree vs. 30 degree and 0 degree vs. 60 degree, respectively.

hours.

3.2 Accuracy of open-loop "tweaking"

The positions of targets in the FoV will change with time after the initial configuration due to differential atmospheric diffraction within the $30'$ FoV and due to the shift of the distortion pattern on the focal plane. The former effect is calculated to be $1.24''$ from zenith to elevation of 60 degree between the top and the bottom of the $30'$ FoV. The cause and details of the latter effect are described in Section 4.2; the size is estimated to be $0.25''$ with a rotation angle change of 13 degrees. The variation of the target relative positions with time limits the maximum integration time after a fiber configuration. If fine-mode step size is stable, the maximum integration can be extended - we can tweak the positions of the fibers in open-loop during integration, i.e. "blindly" move spines a small amount without using the FPI and spine camera for position-feedback.

In order to evaluate the accuracy of the open-loop tweaking, the stability of the step size of the fine mode was measured with numbers of steps of 1, 5, and 10. The results are shown in Fig. 10. The horizontal axis is the average step size of 10 measurements for each step number. The vertical axis shows the differences of the step size in one measurement from the average value normalized to the average step size. For most of the spines, the variation of step size is as small as 20% for 1-step and 10-steps movement. The variation is even smaller for the 5-steps movement. It should be noted that the measurement of the 1-step movement can be significantly affected by the random error of the measurements of spine positions. The results suggest that $\sim 0.5''$ open-loop tweaking can be done with $0.1''$ accuracy.

3.3 Fiber configuration results

The positioning of all 400 science fibers and all 14 guide bundles occurs simultaneously. Firstly, all fibers are moved in an X-direction (positive or negative) using an appropriate (calculated) number of steps for each fiber. The same process is repeated for the Y-direction. Then the positions of all fibers are measured with the spine-camera on the FPI. Initially, all fibers are moved in coarse mode. If the average distance to target is less than

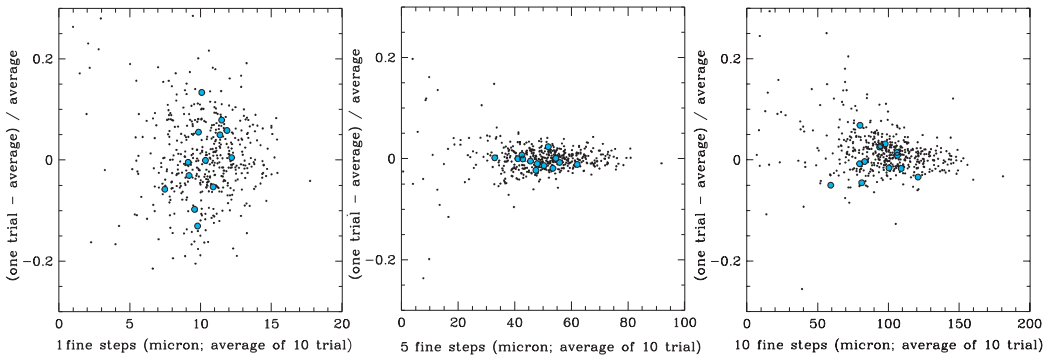

Figure 10. Left) Average spine step size with 1-step fine-mode movement vs. the difference between one measurement and the mean result, i.e. 0.2 corresponds to 20% stepsize variation in one measurement. Middle) for 5-step movement. Right) for 10-step movement.

a threshold value, all of the spines are moved in fine mode during the remaining iteration. The instrument control software (ICS) automatically does the iteration process, based on the fiber allocation data made from a pre-prepared target list. It takes ∼13 minutes to complete 7 iterations; the required configuration time is dominated by the overhead required in moving the FPI to measure the positions of the fibers.

Intensive configuration tests have been performed inside the prime-focus unit at various tilt angles and rotation angles. Two results of the configuration tests are shown in Fig. 10. The top panels show the distribution of the initial distance to the target. The horizontal axis uses a logarithmic scale. The following panels show the distributions after each iteration - the bottom panel showing the result after 7 iterations. For the first configuration test shown on the left, the spines are moved in coarse mode until the third iteration, then 4 iterations in fine mode are performed. In both left and right cases, most of the spines reach within 10μm from the targets after 6 iterations, and about 10 spines do not reach their targets within 10μm even after 7 iterations.

In order to reveal the cause of the large residuals for about 10 spines, we checked the paths of their movement. Fig. 12 shows examples of 6 spines. For each spine, the left panel shows the wide view covering the patrol area, i.e. radius of 7mm, of each spine and the right panel shows the close-up view around its target position marked with large circle indicating 10μm from the target. Starting from the position marked with the blue circle, each spine moved to the red circle going through the positions marked with open circles after each iteration. Although there are a few spines, for example No.361 and No.467 in the figure, that stop moving at a certain point, the paths of other spines suggest that these spines once reach their target position but they are kicked off from the position due to the neighboring spines or due to the vibration caused by the movements of the other spines. For most cases there is no neighbouring spine being positioned on a target close to these spines.

In summary, with a tilt angle <60 degree, 95% of the spines reach target position within 12μm after 7 iterations. Typically, about 10 fibers have difficulty reaching the target positions. At a tilt angle of 60 degrees with some rotation angles, the performance degrades; 90% of the spines reach target position after 7 iterations. The degraded positioning accuracy is because some spines have difficulty moving against gravity.

4. ON SKY COMMISSIONING RESULTS AND PROSPECTS

4.1 Echidna performance at summit and on-sky commissioning

After a thorough evaluation of the fiber positioner at sea level, we brought the Echidna unit to the summit of Mauna Kea and checked the performance again in the low temperature ($\sim$ 5°C), low humidity environment. No degradation of the positioing performance was observed. After installing into the prime-focus unit, Echidna was attached to the top of the telescope. So far, we have conducted on-sky commissioning tests of Echidna on 3 separate occassions - Dec. 2007, Jan. 2008, and May 2008. The results are summarized in the following two subsections.

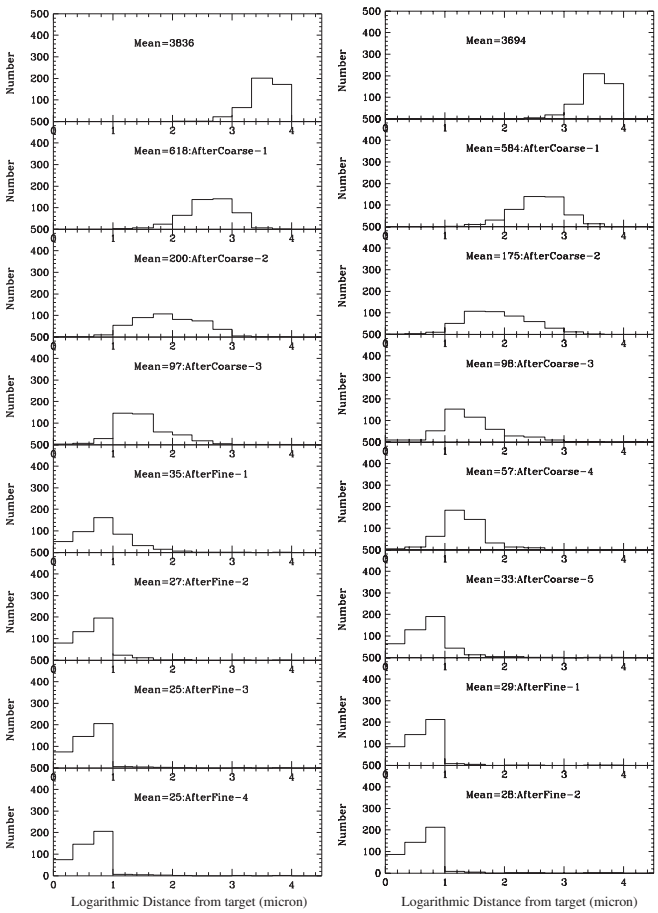

Figure 11. Results of 7-iteration positioning tests from home position to a random position. The horizontal axis shows logarithmic distance from target in microns. Thus 1 and 4 means 10μm and 10mm, respectively. The number of spines as a function of distance from their targets are shown in the histograms.

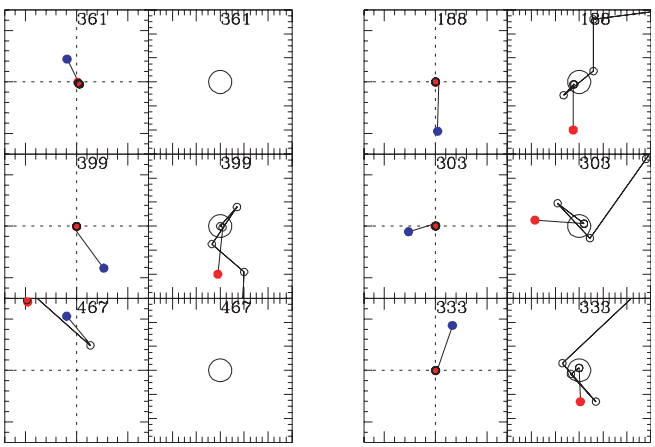

Figure 12. Positioning record of spine residuals larger than 10μm in a positioning test. Left panels are 14mm×14mm fov and right panels are 120μm×120μm fov. The blue points indicate starting position and the red points indicate the final position after 7 iterations. The large circles in the right panels indicate 10μm from the target.

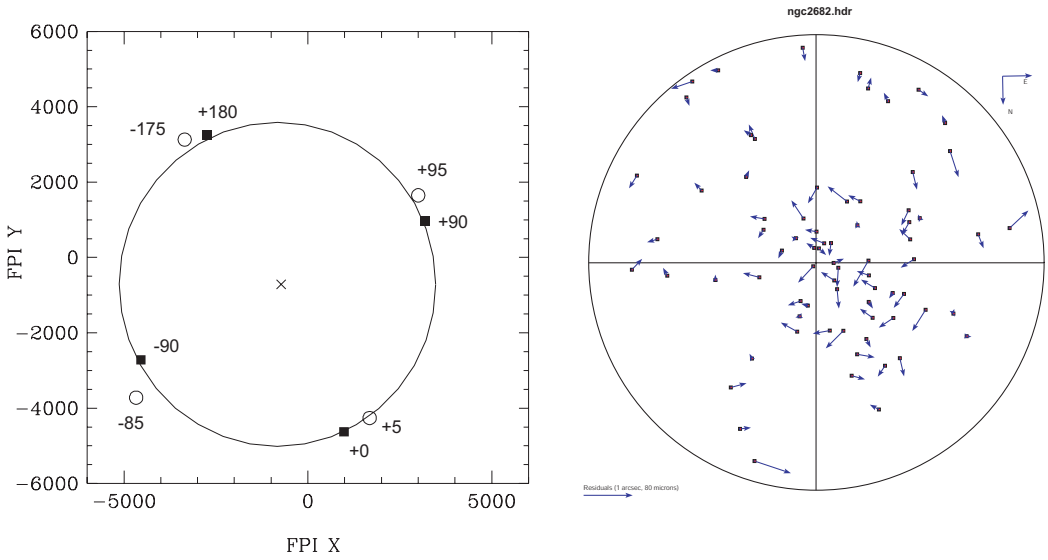

Figure 13. Left) Measured position of the center of the distortion pattern on the focal plane. During the observation, the corrector itself was on the optical axis of the primary mirror. It should be noted that the fibers rotate with the instrument rotator, but the optical axis and the distortion pattern do not. Right) Residual distortion pattern after removing the distortion pattern and the shift of the distortion pattern. Measured in NGC2682. The targets are selected from UCAC2 astrometry catalog.[14] The positional errors are about 20mas for the stars in the 10 to 14 magnitude range, with about 70mas at the limiting magnitude of R about 16 mag.

4.2 Distortion pattern measurements with the sky-camera

The first step of commissioning was the evaluation of the telescope distortion pattern using the sky-camera mounted on the FPI. The sky-camera images the focal plane with $1.3' \times 1.0'$ FoV with $0.1''$ pixel^{-1} image scale. The camera is a non-cooled video-rate CCD with no fore lens system. The camera can detect $R = 15.5$mag stars with averaging 30 frames under relatively bad weather condition; $>1.0''$ FWHM seeing condition with thin cirrus. An OG570 filter is installed in front of the camera to block light shorter than 570nm. Considering the sensitivity curve of the CCD camera, the effective wavelength of the camera is 700nm for objects with flat spectra.

As described in Kimura et al.,[13] there is a offset between the optical axis of the primary mirror and the rotator axis of the instrument rotator. This causes the center of the distortion pattern to move along a circle following the variation of the rotator angle relative to the focal plane of the instrument.

In order to evaluate the distortion pattern and the shift of the center of the pattern against the focal plane, we observed fields with many stars, i.e. open clusters and galactic plane, with the sky-camera. Using measurements taken at various rotator angles, the shift was determined as shown in the left panel of Fig. 13; the center of the distortion pattern moves along a circle with 4.3mm diameter on the focal plane. The center of rotation is consistent with the measured position of the axis of the instrument rotator on the focal plane marked with a cross.

Using the measured distortion pattern and the shift of the center of the pattern against the focal plane, positions of stars on the focal plane can be modelled. The residuals of the current model are shown in the right panel of Fig. 13. The RMS of the residuals is $0.3''$.

4.3 Acquiring stars with the guide-bundles

After the initial refinement of the telescope distortion pattern, we tried acquiring bright stars with the guide-bundles in order to determine the offset between the spine-camera coordinate and the sky-camera coordinate. There are 14 guide-bundles at the right and left edge of the field of view, each covering $78''$ radius area. We expect more than a few stars can be covered even in high-galactic latitude fields above the magnitude limit of

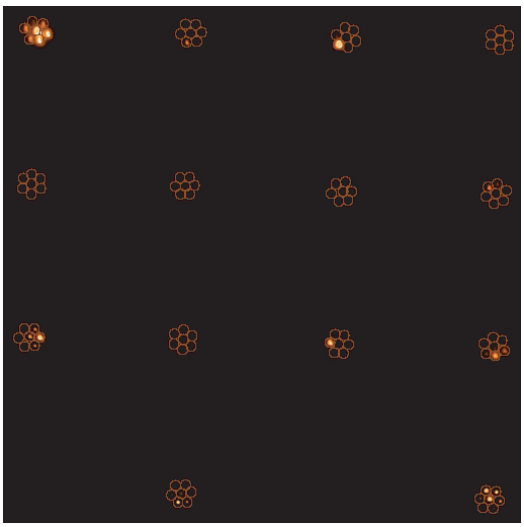

Figure 14. Guide fiber bundle image taken during the May 2008 commissioning run. 10 stars are acquired with the guide bundle. Each bundle consists of 7×50μm diameter fibers. The positions of the 7 fibers of the 14 bundles are marked with circles.

the guide camera ($R = 16 - 18$mag). The output light from the fiber bundles are imaged onto a Hamamatsu water-cooled CCD camera. This camera also has an OG570 filter in front of it.

The result of the acquisition of bright stars with the guide-bundles is shown in Fig. 14. Based on an astrometry catalog in the field, 10 guide-bundle spines are configured to 10 guide stars. After rastering the telescope, the 10 stars were imaged within the FoV of the guide-bundles. Due to the residual of the telescope distortion model, there is a offset between each guide-bundle spine and its guide star and the fiber at the edge is illuminated for most of the guide-bundles.

4.4 Measuring the distortion pattern using the science fibers

The next commissioning observations are scheduled in Jun., Aug., and Oct. in 2008. In order to determine the distortion pattern more accurately, we will use science fibers to map the residual pattern of the current distortion modelling. Initially, fibers will be positioned on targets based on the current distortion modeling and the cataloged positions of stars. Then, "rastering" of the telescope in a grid pattern around the estimated position will enable us to take data with the two spectrographs at each position. Reducing the rastering data, we expect to be able to accurately measure the acquisition error for each science fiber and it's associated target star. With this method, we can sample 400 points inside FoV at once. Furthermore, we can refine the telescope distortion pattern in the observing wavelength directly.

Finally, in Table 1, we summarize the desired and current accuracy of the fiber positioner instrument with a breakdown of the overall error residual into its constituent components: the telescope distortion pattern, the accuracy of the fiber positioning, and the typical uncertainties of the astronomical object catalog. In order to achieve the fiber positioning accuracy of $0.24''$ for most of the fibers as introduced in Introduction, we need to improve the distortion pattern modeling less than $0.05''$ RMS accuracy.

ACKNOWLEDGMENTS

The authors would like to thank all members of the FMOS project, especially, Prof. Toshinori Maihara and Prof. Fumihide Iwamuro. The authors also thank the members of Subaru telescope for their support to the testing of the Echidna unit in the Hilo base and on the telescope, and the members of Anglo-Australian Observatory for their support to complete the instrument.

	Desired			Current		
	($''$)		(μm)	($''$)		(μm)
	RMS	Worst		RMS	Worst	
Distortion pattern modeling	0.05	0.15		0.3	0.9	
Positioning accuracy		0.14	12.0		0.14	12.0
Accuracy of input catalog	0.05	0.15		0.05	0.15	
Total accuracy		0.25			0.9	

Table 1. Summary of the desired and current positioning accuracy of the instrument.

REFERENCES

[1] Maihara, T., Ohta, K., Tamura, N., Ohtani, H., Akiyama, M., et al., "Fiber multi-object spectrograph (fmos) for the subaru telescope," in [*Optical and IR instrumentation and detectors*], Iye, M. and Moorwood, A., eds., *Proc. SPIE* **4008**, 1111–1118 (2000).

[2] Kimura, M., Maihara, T., Ohta, K., Iwamuro, F., Eto, S., Iino., M., Mochida, D., Shima, T., Karoji, H., Noumaru, J., Akiyama, M., et al., "Fibre-multi-object spectrograph (fmos) for subaru telescope," in [*Instrument Design and Performance for Optical/Infrared Ground-based Telescopes*], Iye, M. and Moorwood, A., eds., *Proc. SPIE* **4841**, 974–984 (2003).

[3] Gilligham, P., Miziarsky, S., Akiyama, M., and V.Klocke, "Echidna - a multi-fiber positioner for the subaru telescope," in [*Optical and IR instrumentation and detectors*], Iye, M. and Moorwood, A., eds., *Proc. SPIE* **4008**, 1395–1403 (2000).

[4] Moore, A., Gillingham, P., Griesbach, J., and Akiyama, M., "Spine development for the echidna fiber positioner," in [*Instrument Design and Performance for Optical/Infrared Ground-based Telescopes*], Iye, M. and Moorwood, A., eds., *Proc. SPIE* **4841**, 1429–1439 (2003).

[5] Gilligham, P., Moore, A., Akiyama, M., et al., "The fibre multi-object spectrograph (fmos) project: the anglo-australian observatory role," in [*Instrument Design and Performance for Optical/Infrared Ground-based Telescopes*], Iye, M. and Moorwood, A., eds., *Proc. SPIE* **4841**, 985–996 (2003).

[6] Brzeski, J., Gillingham, P., Correll, D., et al., "Echidna - the engineering challenges," in [*Ground-based Instrumentation for Astronomy*], Moorwood, A. and Iye, M., eds., *Proc. SPIE* **5492**, 1228–1242 (2004).

[7] Eto, S., Maihara, T., Ohta, K., et al., "The fiber multi-object spectrograph (fmos) for the subaru telescope iii," in [*Ground-based Instrumentation for Astronomy*], Moorwood, A. and Iye, M., eds., *Proc. SPIE* **5492**, 1314–1318 (2004).

[8] Iwamuro, F., Maihara, T., Ohta, K., Eto, S., Sakai, M., Akiyama, M., et al., "Fmos - the fiber multiple-object spectrograph iv: current status of ohs-based spectrograph," in [*Ground-based and Airborne Instrumentation for Astronomy*], McLean, I. and Iye, M., eds., *Proc. SPIE* **6269**, 431 (2006).

[9] Lewis, I., Dalton, G., Holmes, A., et al., "Developments on the uk fmos project for the subaru telescope," in [*Instrument Design and Performance for Optical/Infrared Ground-based Telescopes*], Iye, M. and Moorwood, A., eds., *Proc. SPIE* **4841**, 1108–1114 (2003).

[10] Dalton, G., Lewis, I., Bonfield, D., et al., "The uk fmos spectrograph," in [*Ground-based and Airborne Instrumentation for Astronomy*], McLean, I. and Iye, M., eds., *Proc. SPIE* **6269**, 136 (2006).

[11] Murry, G., Woodhouse, G., Froud, T., et al., "An ultraprecision fiber connector for fmos," in [*iber-based Component Fabrication, Testing, and Connectorization*], Pruneri, V., Dahlgren, R., and Gregory, M., eds., *Proc. SPIE* **4943**, 184–194 (2003).

[12] Murry, G., Luke, P., Robertson, D., and Tamura, N., "A connectorized fiber downlink for fmos," *Proc. SPIE* **5492**, 1383–1394 (2004).

[13] Kimura, M., Maihara, T., Iwamuro, F., Eto, S., Akiyama, M., et al., "Fmos: The fiber multi-object spectrograph v results of early pir engineering run," in [*Ground-based and Airborne Instrumentation for Astronomy*], McLean, I. and Iye, M., eds., *Proc. SPIE* **6269**, 132 (2006).

[14] Zacharias, N., Urban, S., Zacharias, M., Wycoff, G., Hall, D., Monet, D., and Rafferty, T., "The second us naval observatory ccd astrograph catalog (ucac2)," *A.J.* **127**, 3043–3059 (2004).